Available online at www.sciencedirect.com

ScienceDirect

Scripta Materialia 70 (2014) 31–34

Scripta MATERIALIA

www.elsevier.com/locate/scriptamat

Microstructure refinement of tungsten by surface deformation for irradiation damage resistance

Mert Efe,[a,d,*] Osman El-Atwani,[a,b] Yang Guo[c,d] and Daniel R. Klenosky[a]

[a]*School of Materials Engineering, Purdue University, West Lafayette, IN, USA*
[b]*School of Nuclear Engineering, Purdue University, West Lafayette, IN, USA*
[c]*School of Industrial Engineering, Purdue University, West Lafayette, IN, USA*
[d]*Center for Materials Processing and Tribology, Purdue University, West Lafayette, IN, USA*

Received 26 April 2013; revised 15 August 2013; accepted 17 August 2013
Available online 23 August 2013

Surface deformation by machining is demonstrated as a way to engineer microstructures of pure tungsten for extreme irradiation environments. Thermomechanical conditions are established for microstructure refinement in the chips and the workpiece subsurface. Ultrafine grains are observed both in the chip and the subsurface, at depths relevant to the typical thickness of the irradiation-induced damage. Guidelines for producing a uniform, ultrafine-grained structure via machining and other surface deformation processes are discussed along with the implications of such microstructures for damage resistance.

Keywords: Surface deformation; Irradiation; Tungsten; Ultrafine grain; Thermomechanical processing

Materials under irradiation fluxes are known to suffer from microstructural damage. One particular and recent example is the surface degradation of plasma-facing tungsten components in experimental fusion reactors. Low-energy helium and hydrogen (<200 eV) ions escaping the plasma can form a surface layer a few micrometers deep consisting of blisters, pores, bubbles and fuzz, which can be detrimental to the operation of the reactor [1]. One approach to mitigate this kind of damage is to refine the microstructure to ultrafine or nanocyrstalline grain sizes. Irradiation-induced defects can be annihilated at the grain boundaries due to the increased area fraction [2]. Crystallographic texture, second-phase precipitates and dislocation density are other potential tools for controlling defects [3,4].

While powder metallurgy [4,5] and severe plastic deformation techniques [6–8] are successful in modifying the microstructure of the whole bulk material, surface deformation techniques such as machining [9,10], ultrasonic shot peening [11], sliding [12,13] and friction stir processing [14] can be efficient alternatives. The typical thickness ($\geqslant$50 μm) of the deformed layers possible with these processes correlates well with the length scale of surface damage due to helium irradiation (up to several microns) under fusion-relevant conditions [1].

In this study, we demonstrate machining as a way to engineer the surface microstructure of pure tungsten by controlling the thermomechanical conditions during the deformation. Commercial-purity tungsten (99.95%) in disk form (American Elements, Los Angeles, CA) was subjected to plane strain, extrusion machining [15] as shown in Figure 1. A sharp, wedge-shaped cutting tool with a rake angle of α removes a preset thickness (t_o, also called the undeformed chip thickness) and width (t_w) of material in the form of a chip, by imposing large shear strains in a narrow and confined deformation zone. The final chip thickness, t_c, is set a priori before the machining by the constraining tool, which allows a fixed chip thickness ratio of $\lambda = t_c/t_0$. Tungsten carbide cutting and constraining tools with 0.8 mm edge radius (SPG 422 type) were used for machining without application of any coolant.

The strain and strain rate in the deformation zone and the subsurface is measured using particle image velocimetry (PIV), a correlation-based image analysis technique [9]. PIV was applied to 70/30 brass alloy, which models the deformation field in tungsten. Previous PIV work in other materials such as titanium,

* Corresponding author at: School of Materials Engineering, Purdue University, West Lafayette, IN, USA. Tel.: +90 555 345 1515; e-mail: mefe@purdue.edu

1359-6462/$ - see front matter © 2013 Acta Materialia Inc. Published by Elsevier Ltd. All rights reserved.
http://dx.doi.org/10.1016/j.scriptamat.2013.08.013

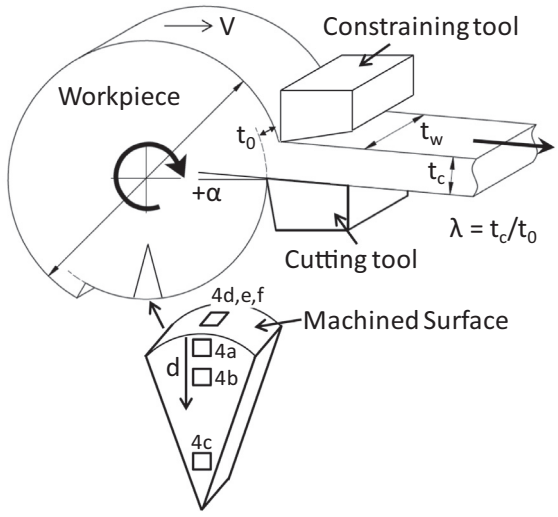

Figure 1. Schematic drawing of plane strain, extrusion machining. Location of the FIB images (Fig. 4) are shown on the inset, where d represents the distance from the machined surface.

copper and lead showed that the strain accumulated in the chip is mostly independent of the material system and depends solely on λ and α [9,15,16]. Moreover, both materials yield a similar value of $\lambda \approx 3.5$ at $\alpha = 0$ when machined without the constraining tool. This being an indication of similar deformation fields, tungsten is machined at $\alpha = 0$ and $\lambda = 3$ in order to match the experimental conditions in the PIV analysis of brass.

Figure 2a shows the effective strain rate ($d\bar{\varepsilon}/dt$) field during the machining. The region of intense strain rate represents the narrow deformation zone having an average thickness (Δ) of ~100 μm. The chip and the very surface it has just separated from (i.e. the machined surface) experience a similar deformation history. The machined surface ($d \approx 0$ μm) also enters the deformation zone and accumulates the same amount of strain (Fig. 2a). This effective strain is obtained by integrating the effective strain rate along the pathline of the material flow. Figure 2b shows the accumulation of strain in the chip and the subsurface ($d = 10$ μm) along paths 1 and 2, respectively. The final strain in the chip and the machined surface ($\bar{\varepsilon} = 2.1$) drops sharply (to $\bar{\varepsilon} = 1.2$) at 10 μm depth.

The effective strain imposed in the chip and the machined surface, $\bar{\varepsilon}_s$, can also be calculated relatively accurately by idealizing the deformation zone as a single shear plane [9]. The effective strain, in this case, is:

$$\bar{\varepsilon}_s = \frac{1}{\sqrt{3}}\left(\frac{\lambda}{\cos\alpha} + \frac{1}{\lambda\cos\alpha} - 2\tan\alpha\right). \quad (1)$$

The experimental parameters used in this study, $\alpha = 0$ and $\lambda = 3$, resulted in $\bar{\varepsilon}_s = 1.9$, which is close to the PIV measurements. Previous work on various material systems also confirmed the correlation between the shear plane model and the PIV for $\lambda > 1$ [9,15,16], justifying the use of Eq. (1) to estimate $\bar{\varepsilon}_s$.

An exponential decay of strain with depth into the workpiece can be predicted based on the PIV measurements:

$$\bar{\varepsilon}_d = \bar{\varepsilon}_s \exp\left(\frac{-k_\alpha d}{t_0}\right), \quad (2)$$

where d is the distance from the machined surface and k_α is a parameter that only depends on α [9]. Eq. (2) is plotted for various rake angles at $t_0 = 0.125$ mm (Fig. 2c). The constant, k_α, is assumed to be 8 for $\alpha = 0$ and 6.5 for $\alpha = -20$, based on the experimental results [9]. While $\bar{\varepsilon}_s$ is increasing with more negative α values, the depth of the deformed layer is controlled by both α and t_0. Therefore, a combination of negative α and large t_0 is ideal for thick deformed layers with the highest possible strain. Burnishing, sliding and surface grinding treatment are examples of processes that can satisfy these conditions [12,13,17,18].

The strain rate and the temperature of the deformation zone (T) can be controlled as well as the strain, and these are primarily determined by the deformation speed (i.e. the surface speed of the disk), V [15]. The relation of the strain rate to the deformation speed is given by: $\dot{\bar{\varepsilon}} \sim \bar{\varepsilon}V/\Delta$, resulting in a large range of strain rate $10 < \dot{\bar{\varepsilon}} < 10^5$ via V (~1 mm/s to 6 m/s). The process also becomes adiabatic as V increases. The heat generated during the plastic deformation stays in the deformation zone with increasing adiabadicity. Thus, the temperature

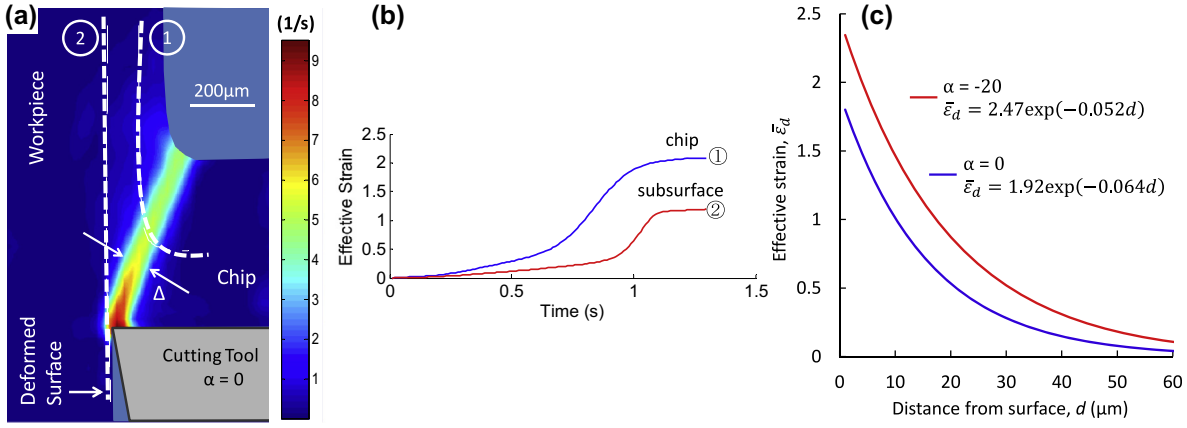

Figure 2. PIV analysis of machining showing (a) strain-rate field and (b) accumulation of effective strain along the chip and the subsurface. Work material is 70/30 brass, with machining conditions of $\alpha = 0$, $t_0 = 0.150$ mm, $\lambda = 3.4$, and $V = 1$ mm s^{-1}. (c) Variation of the subsurface strain with d (Eq. (2)).